

# Magnetism from Conductors and Enhanced Nonlinear Phenomena

J. B. Pendry, A. J. Holden, D. J. Robbins, and W. J. Stewart, *Member, IEEE*

**Abstract**—We show that microstructures built from nonmagnetic conducting sheets exhibit an effective magnetic permeability  $\mu_{\text{eff}}$ , which can be tuned to values not accessible in naturally occurring materials, including large imaginary components of  $\mu_{\text{eff}}$ . The microstructure is on a scale much less than the wavelength of radiation, is not resolved by incident microwaves, and uses a very low density of metal so that structures can be extremely lightweight. Most of the structures are resonant due to internal capacitance and inductance, and resonant enhancement combined with compression of electrical energy into a very small volume greatly enhances the energy density at critical locations in the structure, easily by factors of a million and possibly by much more. Weakly nonlinear materials placed at these critical locations will show greatly enhanced effects raising the possibility of manufacturing active structures whose properties can be switched at will between many states.

**Index Terms**—Effective permeability, nonlinearity, photonic crystals.

## I. INTRODUCTION

IN A SENSE, every material is a composite, even if the individual ingredients consist of atoms and molecules. The original objective in defining a permittivity  $\epsilon$  and permeability  $\mu$  was to present an homogeneous view of the electromagnetic properties of a medium. Therefore, it is only a small step to replace the atoms of the original concept with structure on a larger scale. We shall consider periodic structures defined by a unit cell of characteristic dimensions  $a$ . The contents of the cell will define the effective response of the system as a whole.

Clearly, there must be some restrictions on the dimensions of the cell. If we are concerned about the response of the system to electromagnetic radiation of frequency  $\omega$ , the conditions are easy to define as follows:

$$a \ll \lambda = 2\pi c_0 \omega^{-1}. \quad (1)$$

If this condition were not obeyed, there would be the possibility that internal structure of the medium could diffract as well as refract radiation giving the game away immediately. Long wavelength radiation is too myopic to detect internal structure and, in this limit, an effective permittivity and permeability is a valid concept. In Section II, we shall discuss how the microstructure can be related to  $\epsilon_{\text{eff}}$ ,  $\mu_{\text{eff}}$ .

In an earlier paper [1], we showed how a structure consisting of very thin infinitely long metal wires arranged in a three-

dimensional (3-D) cubic lattice could model the response of a dilute plasma, giving a negative  $\epsilon_{\text{eff}}$  below a plasma frequency somewhere in the gigahertz range. Theoretical analysis of this structure has been confirmed by experiment [2]. Sievenpiper *et al.* have also investigated plasma-like effects in metallic structures [3], [4].

Ideally, we should like to proceed in the magnetic case by finding the magnetic analogue of a good electrical conductor: unfortunately, there is not one. Nevertheless, we can find some alternatives that we believe do give rise to interesting magnetic effects.

Why should we go to the trouble of microstructuring a material simply to generate a particular  $\mu_{\text{eff}}$ ? The answer is that atoms and molecules prove to be a rather restrictive set of elements from which to build a magnetic material. This is particularly true at frequencies in the gigahertz range where the magnetic response of most materials is beginning to tail off. Those materials, such as the ferrites, that remain moderately active are often heavy, and may not have very desirable mechanical properties. In contrast, we shall show, microstructured materials can be designed with considerable magnetic activity, both diamagnetic and paramagnetic, and can, if desired, be made extremely light.

There is another quite different motivation. We shall see that strong magnetic activity implies strongly inhomogeneous fields inside the material. In some instances, this may result in local field strengths many orders of magnitude larger than in free space. Doping the composite with nonlinear material at the critical locations of field concentration gives enhanced nonlinearity, reducing power requirements by the field enhancement factor. This is not an option available in a conventional magnetic material.

We show first how to calculate  $\mu_{\text{eff}}$  for a system, then we propose some model structures that have magnetic activity and give some numbers for these systems. Finally, we show how electrostatic energy can be strongly concentrated in these structures and, hence, demonstrate the potential for enhancing nonlinear effects.

## II. DEFINING AN EFFECTIVE PERMEABILITY

We are seeking to build structures with effective epsilon and  $\mu$  as follows:

$$\begin{aligned} \mathbf{B}_{\text{ave}} &= \mu_{\text{eff}} \mu_0 \mathbf{H}_{\text{ave}} \\ \mathbf{D}_{\text{ave}} &= \epsilon_{\text{eff}} \epsilon_0 \mathbf{E}_{\text{ave}} \end{aligned} \quad (2)$$

where we assume that the structure is on a scale much shorter than the wavelength of any radiation so that we can sensibly

Manuscript received March 8, 1999; revised July 9, 1999.  
J. B. Pendry is with The Blackett Laboratory, Imperial College, London SW7 2BZ, U.K.

A. J. Holden, D. J. Robbins, and W. J. Stewart are with GEC-Marconi Materials Technology Ltd, Caswell, Towcester, NN12 8EQ, U.K.

Publisher Item Identifier S 0018-9480(99)08781-5.

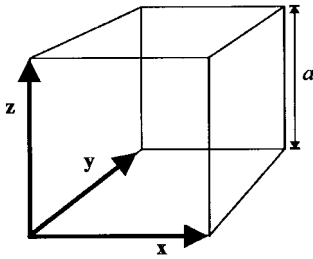


Fig. 1. Unit cell of a periodic structure. We assume that the unit cell dimensions are much smaller than the wavelength of radiation, and average over local variations of the fields. In the case of the  $\mathbf{B}$ -field, we average over the faces of the cell and in the case of the  $\mathbf{H}$ -field, over one of the edges.

speak of an average value for all the fields. A key question is “how do the averages differ?” Clearly, if the structure is made of *thin* wires or sheets of metal, then if the averages were taken over the same regions of space,  $\epsilon_{\text{eff}}$ ,  $\mu_{\text{eff}}$  would always be unity. However, we observe that Maxwell’s equations

$$\begin{aligned}\nabla \times \mathbf{H} &= +\partial \mathbf{D} / \partial t \\ \nabla \times \mathbf{E} &= -\partial \mathbf{B} / \partial t\end{aligned}\quad (3)$$

may be applied in the integral form

$$\begin{aligned}\int_c \mathbf{H} \cdot d\mathbf{l} &= +\frac{\partial}{\partial t} \int_s \mathbf{D} \cdot d\mathbf{S} \\ \int_c \mathbf{E} \cdot d\mathbf{l} &= -\frac{\partial}{\partial t} \int_s \mathbf{B} \cdot d\mathbf{S}\end{aligned}\quad (4)$$

where the line integral is taken over a loop “ $c$ ,” which encloses an area “ $s$ .”

This form of the equations immediately suggests a prescription for averaging the fields. For simplicity, we shall assume that the periodic structure is described by a unit cell whose axes are orthogonal, as shown in Fig. 1. Some of the arguments used in this section are similar to those we used in deriving a finite-difference model of Maxwell’s equations [5].

We choose to define the components of  $\mathbf{H}_{\text{ave}}$  by averaging the  $\mathbf{H}$ -field along each of the three axes of the unit cell. If we assume a simple cubic system

$$\begin{aligned}(H_{\text{ave}})_x &= a^{-1} \int_{\mathbf{r}=(0,0,0)}^{\mathbf{r}=(a,0,0)} \mathbf{H} \cdot d\mathbf{r} \\ (H_{\text{ave}})_y &= a^{-1} \int_{\mathbf{r}=(0,0,0)}^{\mathbf{r}=(0,a,0)} \mathbf{H} \cdot d\mathbf{r} \\ (H_{\text{ave}})_z &= a^{-1} \int_{\mathbf{r}=(0,0,0)}^{\mathbf{r}=(0,0,a)} \mathbf{H} \cdot d\mathbf{r}.\end{aligned}\quad (5)$$

There is only one caveat concerning the definition of the unit cell: its edges must not intersect with any of the structures contained within the unit cell. This leaves us free to cut the structure into a whole number of unit cells when we come to create a surface and ensures that the parallel component of  $\mathbf{H}_{\text{ave}}$  is continuous across the surface as required in a consistent theory of an effective medium.

To define  $\mathbf{B}_{\text{ave}}$ , we average the  $\mathbf{B}$ -field over each of the three faces of the unit cell, defined as follows:

- $S_x$  surface defined by the vectors  $\mathbf{y}$ ,  $\mathbf{z}$ ;
- $S_y$  surface defined by the vectors  $\mathbf{x}$ ,  $\mathbf{z}$ ;

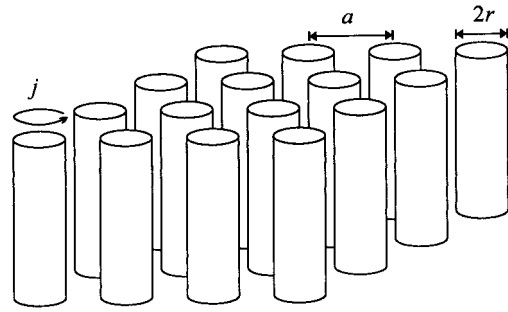


Fig. 2. Model A consists of a square array of metallic cylinders designed to have magnetic properties in the direction parallel to the axes of the cylinders.

$S_z$  surface defined by the vectors  $\mathbf{x}$ ,  $\mathbf{y}$ .

Hence, we define

$$\begin{aligned}(B_{\text{ave}})_x &= a^{-2} \int_{S_x} \mathbf{B} \cdot d\mathbf{S} \\ (B_{\text{ave}})_y &= a^{-2} \int_{S_y} \mathbf{B} \cdot d\mathbf{S} \\ (B_{\text{ave}})_z &= a^{-2} \int_{S_z} \mathbf{B} \cdot d\mathbf{S}.\end{aligned}\quad (6)$$

The ratio defines the effective epsilon and  $\mu$  from (2)

$$\begin{aligned}(\mu_{\text{eff}})_x &= (B_{\text{ave}})_x / (\mu_0 H_{\text{ave}})_x \\ (\mu_{\text{eff}})_y &= (B_{\text{ave}})_y / (\mu_0 H_{\text{ave}})_y \\ (\mu_{\text{eff}})_z &= (B_{\text{ave}})_z / (\mu_0 H_{\text{ave}})_z.\end{aligned}\quad (7)$$

Thus, if we seek a large effect, we must try to create fields that are as inhomogeneous as possible.

We shall explore various configurations of thin sheets of metal, derive  $\mu_{\text{eff}}$ , and discuss the results with a view to making the effect as large as possible.

### III. EXAMPLES OF MAGNETIC MICROSTRUCTURES

#### A. An Array of Cylinders

We start with a very simple structure for the purposes of illustration, i.e., “model A” shown in Fig. 2. Let us apply an external field  $H_0$ , which we shall take to be parallel to the cylinders. We assume that the cylinders have a conducting surface so that a current  $j$  per unit length flows. The field inside the cylinders is

$$\mathbf{H} = H_0 + j - \frac{\pi r^2}{a^2} j \quad (8)$$

where the second term on the right-hand side is the field caused directly by the current, and the third term is the result of the depolarizing fields with sources at the remote ends of the cylinders. If the cylinders are very long, the depolarizing field will be uniformly spread over the unit cell, but will have the same number of lines of force in it as the direct field inside the cylinders. We now calculate the total electromotive force

(emf) around the circumference of a cylinder as follows:

$$\begin{aligned} \text{emf} &= -\pi r^2 \mu_0 \frac{\partial}{\partial t} \left[ H_0 + j - \frac{\pi r^2}{a^2} j \right] - 2\pi r \sigma j \\ &= +i\omega \pi r^2 \mu_0 \left[ H_0 + j - \frac{\pi r^2}{a^2} j \right] - 2\pi r \sigma j \end{aligned} \quad (9)$$

where  $\sigma$  is the resistance of the cylinder surface per unit area. The net emf must balance and, therefore,

$$j = \frac{-i\omega \pi r^2 \mu_0 H_0}{i\omega \pi r^2 \mu_0 \left[ 1 - \frac{\pi r^2}{a^2} \right] - 2\pi r \sigma} = \frac{-H_0}{\left[ 1 - \frac{\pi r^2}{a^2} \right] + i \frac{2r\sigma}{\omega r^2 \mu_0}}. \quad (10)$$

We are now in a position to calculate the relevant averages. The average of the  $B$ -field over the entire unit cell is

$$B_{\text{ave}} = \mu_0 H_0. \quad (11)$$

However, if we average the  $H$ -field over a line lying entirely outside the cylinders

$$\begin{aligned} H_{\text{ave}} &= H_0 - \frac{\pi r^2}{a^2} j \\ &= H_0 - \frac{\pi r^2}{a^2} \frac{-H_0}{\left[ 1 - \frac{\pi r^2}{a^2} \right] + i \frac{2r\sigma}{\omega r^2 \mu_0}} \\ &= H_0 \frac{1 + i \frac{2\sigma}{\omega r \mu_0}}{\left[ 1 - \frac{\pi r^2}{a^2} \right] + i \frac{2\sigma}{\omega r \mu_0}}. \end{aligned} \quad (12)$$

Hence, we define

$$\begin{aligned} \mu_{\text{eff}} &= \frac{B_{\text{ave}}}{\mu_0 H_{\text{ave}}} \\ &= \frac{1 - \frac{\pi r^2}{a^2} + i \frac{2\sigma}{\omega r \mu_0}}{1 + i \frac{2\sigma}{\omega r \mu_0}} \\ &= 1 - \frac{\pi r^2}{a^2} \left[ 1 + i \frac{2\sigma}{\omega r \mu_0} \right]^{-1}. \end{aligned} \quad (13)$$

For an infinitely conducting cylinder or in the high frequency limit,  $\mu_{\text{eff}}$  is reduced by the ratio of the cylinder volume to the cell volume. This ratio of volumes will turn out to be the key factor in determining the strength of the effect in all our models. Evidently, in the present model,  $\mu_{\text{eff}}$  can never be less than zero or greater than unity. It should also be mentioned that to maximize the effect, we could have replaced the metallic cylinders with prisms of square cross section to maximize the volume enclosed within the prism.

If the resistivity of the sheets is high, then the additional contribution to  $\mu_{\text{eff}}$  is imaginary, but always less than unity

$$\mu_{\text{eff}} \approx 1 + i \frac{\pi r^3 \omega \mu_0}{2\sigma a^2}, \quad \sigma \gg \omega r \mu_0. \quad (14)$$

A further point that should be noted is that all the structures we discuss have electrical as well as magnetic properties. In

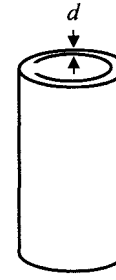


Fig. 3. Model  $B$  consists of a square array of cylinders as for model  $A$ , but with the difference that the cylinders now have internal structure. The sheets are divided into a “split ring” structure and separated from each other by a distance  $d$ . In any one sheet, there is a gap that prevents current from flowing around that ring.

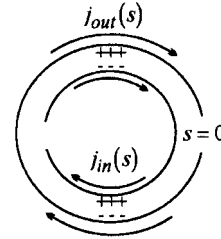


Fig. 4. When a magnetic field parallel to the cylinder is switched on it induces currents in the “split rings,” as shown here. The greater the capacitance between the sheets, the greater the current.

this particular case, we can crudely estimate for electric fields perpendicular to the cylinders

$$\epsilon_{\text{eff}} = (1 - F)^{-1} = \left( 1 - \frac{\pi r^2}{a^2} \right)^{-1} \quad (15)$$

where  $F$  is the fraction of the structure not internal to a cylinder. In deriving (15), we assume that the cylinder is a perfect conductor and neglect depolarizing fields arising from interaction between cylinders. Inclusion of  $\epsilon_{\text{eff}}$  in our calculations removes one difficulty by ensuring that

$$\lim_{\omega \rightarrow \infty} c_{\text{light}} = \lim_{\omega \rightarrow \infty} c_0 (\epsilon_{\text{eff}} \mu_{\text{eff}})^{-(1/2)} = c_0. \quad (16)$$

Evidently, without  $\epsilon_{\text{eff}}$  the velocity of light in the effective medium would have exceeded that in free space. Most of the structures discussed in this paper have a similar  $\epsilon_{\text{eff}}$ .

### B. Capacitative Array of Sheets Wound on Cylinders

The previous structure showed a limited magnetic effect. We now show how to extend the range of magnetic properties available to us by introducing capacitive elements into the structure. We take the same structure of cylinders as before, except that the cylinders are now built in a “split ring” configuration, as shown in Fig. 3.

The important point is that there is a gap that prevents current from flowing around any one ring. However, there is a considerable capacitance between the two rings, which enables current to flow (see Fig. 4).

Detailed calculations give

$$\mu_{\text{eff}} = 1 - \frac{F}{1 + \frac{2\sigma i}{\omega r \mu_0} - \frac{3}{\pi^2 \mu_0 \omega^2 C r^3}} \quad (17)$$

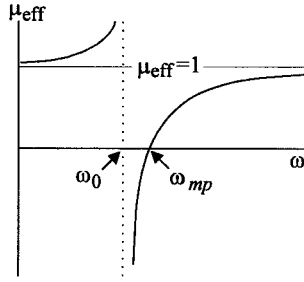


Fig. 5. The effective magnetic permeability for model *B* shows a resonant structure dictated by the capacitance between the sheets and magnetic inductance of the cylinder. We sketch the typical form of a highly conducting sample,  $\sigma \approx 0$ . Below the resonant frequency,  $\mu_{\text{eff}}$  is enhanced, but above resonance,  $\mu_{\text{eff}}$  is less than unity and may be negatively close to the resonance.

where  $F$  is the fractional volume of the cell occupied by the interior of the cylinder

$$F = \frac{\pi r^2}{a^2} \quad (18)$$

and  $C$  is the capacitance per unit area between the two sheets

$$C = \frac{\varepsilon_0}{d} = \frac{1}{dc_0^2 \mu_0}. \quad (19)$$

Hence,

$$\mu_{\text{eff}} = 1 - \frac{\frac{\pi r^2}{a^2}}{1 + \frac{2\sigma i}{\omega r \mu_0} - \frac{3dc_0^2}{\pi^2 \omega^2 r^3}}. \quad (20)$$

Since we now have capacitance in the system that can balance the inductance present,  $\mu_{\text{eff}}$  has a resonant form, which is sketched in Fig. 5.

Fig. 5 illustrates the generic form of  $\mu_{\text{eff}}$  for all the structures we present here.

We define  $\omega_0$  to be the frequency at which  $\mu_{\text{eff}}$  diverges as follows:

$$\omega_0 = \sqrt{\frac{3}{\pi^2 \mu_0 C r^3}} = \sqrt{\frac{3dc_0^2}{\pi^2 r^3}} \quad (21)$$

and  $\omega_{mp}$  to be the “magnetic plasma frequency”

$$\omega_{mp} = \sqrt{\frac{3}{\pi^2 \mu_0 C r^3 (1-F)}} = \sqrt{\frac{3dc_0^2}{\pi^2 r^3 \left(1 - \frac{\pi r^2}{a^2}\right)}}. \quad (22)$$

Note that the separation between  $\omega_0$  and  $\omega_{mp}$ , which is a measure of the range of frequencies over which we see a strong effect, is determined by

$$F = 1 - \frac{\pi r^2}{a^2} \quad (23)$$

the fraction of the structure not internal to a cylinder. As for the case *A*, the simple cylinder, the high frequency limit is given by

$$\lim_{\omega \rightarrow \infty} \mu_{\text{eff}}(\omega) = 1 - \frac{\pi r^2}{a^2}. \quad (24)$$

We mention in passing that the system sustains longitudinal magnetic modes at the magnetic plasma frequency, the analog

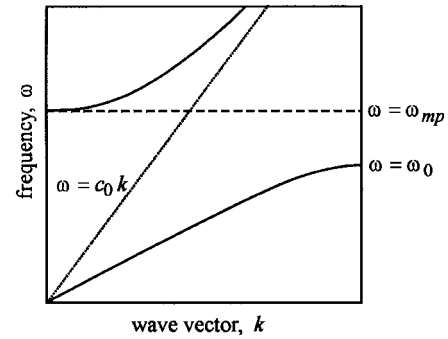


Fig. 6. Generic dispersion relationship for resonant structures with a  $\mu_{\text{eff}}$ . The solid lines represent twofold degenerate transverse modes and the dashed line a single longitudinal magnetic plasmon mode.

of the plasma modes of a gas of free electrical charges [6], [7]. Of course, we have no free magnetic poles, only the appearance of such as currents around the cylinders make the cylinder ends appear to support free magnetic poles in the fashion of a bar magnet.

Together with  $\varepsilon_{\text{eff}}$ , given in (15), which is also applicable here, we can illustrate a generic dispersion relationship, as shown in Fig. 6.

The relevant points to note are as follows.

- 1) Wherever  $\mu_{\text{eff}}$  is negative there is a gap in the dispersion relationship, i.e., for

$$\omega_0 < \omega < \omega_{mp}. \quad (25)$$

- 2) A longitudinal magnetic plasma mode, dispersionless in this approximation, is seen at  $\omega = \omega_{mp}$ .
- 3) The dispersion relation converges asymptotically to the free-space light cone, as discussed above. In fact, metallic structures in general represent a fresh approach to the photonic insulator concept introduced independently by Yablonovitch [8], [9] and John [10].

If we take the following values:

$$\begin{aligned} r &= 2.0 \times 10^{-3} \text{ m} \\ a &= 5.0 \times 10^{-3} \text{ m} \\ d &= 1.0 \times 10^{-4} \text{ m} \end{aligned} \quad (26)$$

we get

$$f_{mp} = (2\pi)^{-1} \omega_{mp} = 4.17 \times 10^9 \text{ Hz} \quad (27)$$

$$f_0 = f_{mp} \sqrt{\left(1 - \frac{\pi r^2}{a^2}\right)} = 2.94 \times 10^9 \text{ Hz}. \quad (28)$$

Note that the frequency at which the structure is active corresponds to a free-space wavelength of 10 cm, much greater than the 0.5-cm separation between cylinders. This will be typical of these capacitive structures and implies that the effective medium approximation will be excellent.

### C “Swiss Roll” Capacitor

We take the same arrangement of cylinders on a square lattice as before, except that the cylinders are now build as shown in Fig. 7. The important point is again that no



Fig. 7. In model *C*, a metallic sheet is wound around each cylinder in a coil. Each turn of the coil is spaced by a distance  $d$  from the previous sheet.

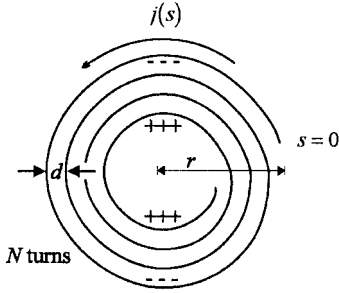


Fig. 8. When a magnetic field parallel to the cylinder is switched on, it reduces currents in the coiled sheets, as shown here. Capacitance between the first and last turns of the coil enables the current to flow.

current can flow around the coil, except by virtue of the self capacitance (see Fig. 8).

In this instance, we find for the effective permeability

$$\begin{aligned} \mu_{\text{eff}} &= 1 - \frac{F}{1 + \frac{2\sigma i}{\omega r \mu_0 (N-1)} - \frac{1}{2\pi^2 r^3 \mu_0 (N-1)^2 \omega^2 C}} \\ &= 1 - \frac{\frac{\pi r^2}{a^2}}{1 + \frac{2\sigma i}{\omega r \mu_0 (N-1)} - \frac{dc_0^2}{2\pi^2 r^3 (N-1)\omega^2}} \end{aligned} \quad (29)$$

where  $F$  is as before the fraction of the structure not internal to a cylinder, and the capacitance per unit area between the first and the last of the coils is

$$C = \frac{\epsilon_0}{d(N-1)} = \frac{1}{\mu_0 dc_0^2 (N-1)}. \quad (30)$$

The critical frequencies are

$$\begin{aligned} \omega_0 &= \sqrt{\frac{1}{2\pi^2 r^3 \mu_0 C (N-1)^2}} \\ &= \sqrt{\frac{dc_0^2}{2\pi^2 r^3 (N-1)}} \end{aligned} \quad (31)$$

$$\begin{aligned} \omega_{mp} &= \sqrt{\frac{1}{F 2\pi^2 r^3 \mu_0 C (N-1)^2}} \\ &= \sqrt{\frac{dc_0^2}{\left(1 - \frac{\pi r^2}{a^2}\right) 2\pi^2 r^3 (N-1)}}. \end{aligned} \quad (32)$$

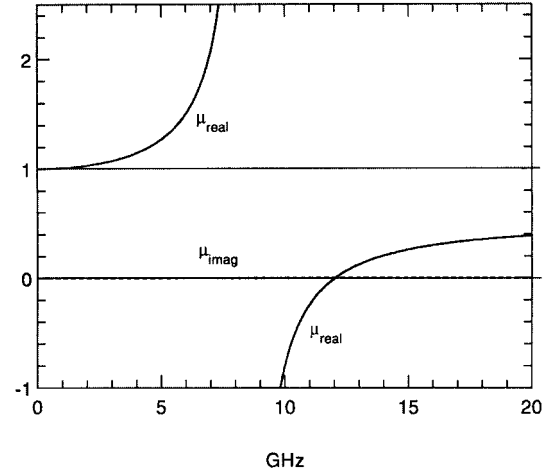


Fig. 9. Dispersion with frequency of  $\mu_{\text{eff}}$  for a Swiss roll structure, calculated for the parameters shown in (36), assuming that the metal has zero resistivity.

If we take the values we used before in (26)

$$\begin{aligned} r &= 2.0 \times 10^{-3} \text{ m} \\ a &= 5.0 \times 10^{-3} \text{ m} \\ d &= 1.0 \times 10^{-4} \text{ m} \\ N &= 11 \end{aligned} \quad (33)$$

we get

$$f_0 = (2\pi)^{-1} \omega_0 = 0.380 \times 10^9 \text{ Hz} \quad (34)$$

$$f_{mp} = (2\pi)^{-1} \omega_{mp} = 0.539 \times 10^9 \quad (35)$$

i.e., there is much more capacitance in this model and the range of active frequencies is an order of magnitude lower than it was in model *C*, which used only two overlapping sheets.

Choosing an even smaller scale and reducing the number of turns in order to drive up the frequencies to our range of interest

$$\begin{aligned} r &= 2.0 \times 10^{-4} \text{ m} \\ a &= 5.0 \times 10^{-4} \text{ m} \\ d &= 1.0 \times 10^{-5} \text{ m} \\ N &= 3 \end{aligned} \quad (36)$$

we get

$$f_0 = 8.50 \times 10^9 \text{ Hz} \quad (37)$$

$$f_{mp} = 12.05 \times 10^9 \text{ Hz}. \quad (38)$$

Note that the free-space wavelength at the plasma frequency is around 3 cm, and compare this to the very much smaller spacing between cylinders of 0.05 cm.

We shall now calculate the dispersion of  $\mu_{\text{eff}}$  for various parameters. First let us take the parameters given in (36). The resulting dispersion of  $\mu_{\text{eff}}$  is shown in Fig. 9.

We next enquire ‘‘what is the effect of making the sheets resistive?’’ Below we present a series of calculations for various values of the resistivity  $\sigma$  given in  $\Omega$ .

In Fig. 10, we increase the resistivity from 0.1 to 10.0  $\Omega$ . Note the broadening of the resonance, the complementary

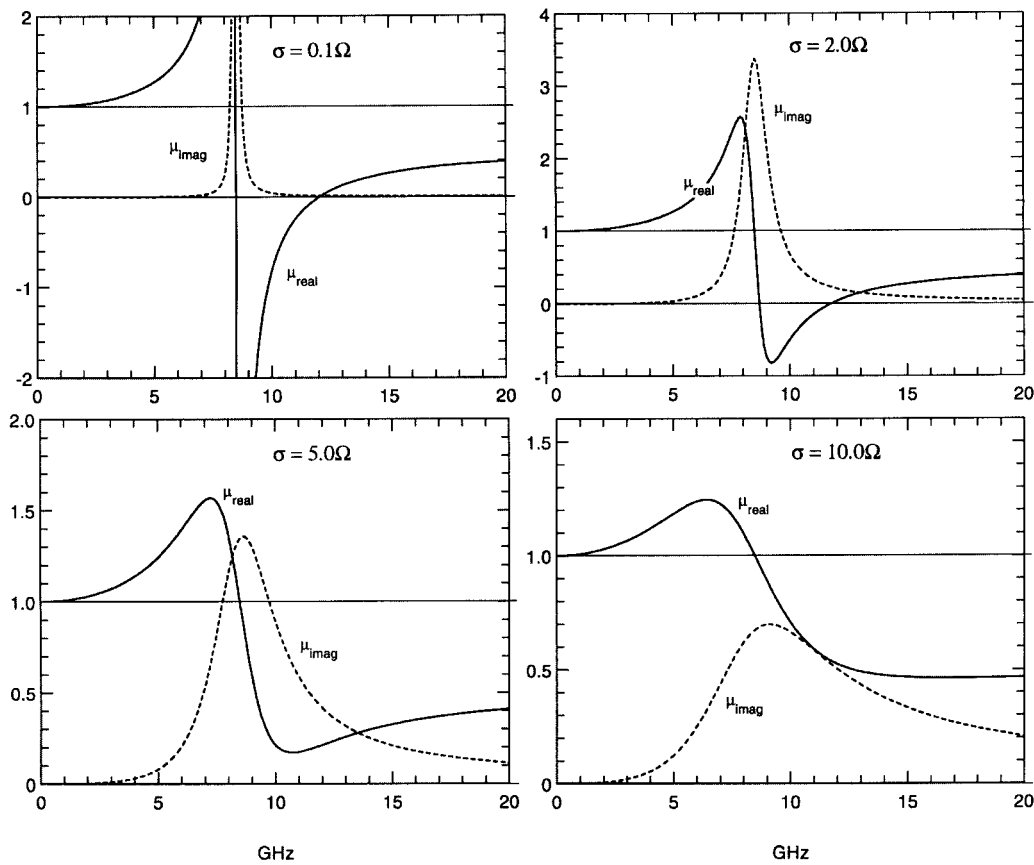


Fig. 10. Dispersion with frequency of  $\mu_{\text{eff}}$  for a Swiss roll structure, calculated for the parameters shown in (36), for various values of the resistivity of the sheets: 0.1, 2.0, 5.0, 10.0  $\Omega$ .

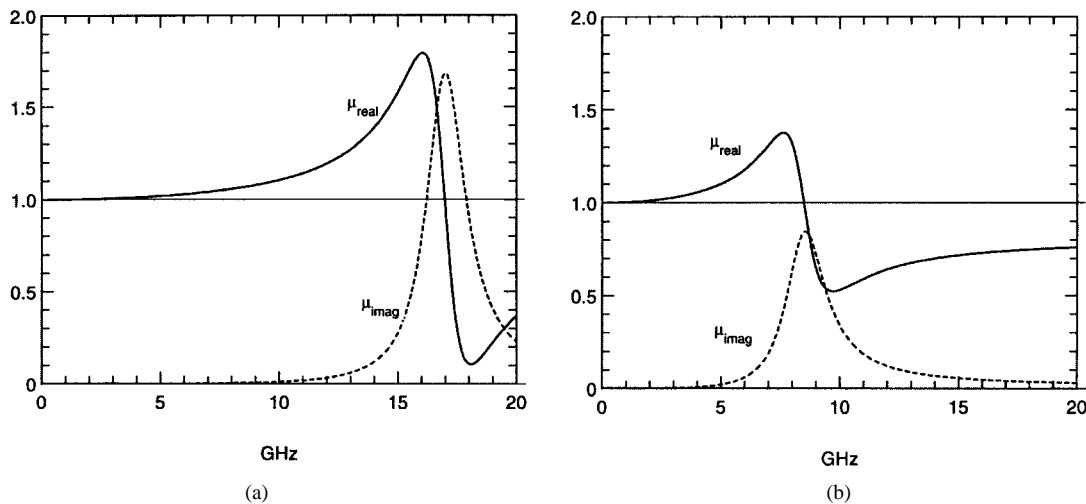


Fig. 11. Dispersion with frequency of  $\mu_{\text{eff}}$  for a Swiss roll structure. (a) Calculated for the parameters shown in (36), except that the resistivity of the sheets is now 2.0  $\Omega$ , and the radius of the cylinders has been reduced from  $2.0 \times 10^{-4}$  to  $12.6 \times 10^{-4}$  m, thus raising the resonant frequency by a factor of two. (b):  $d$ , the spacing between the sheets, has been reduced to  $0.25 \times 10^{-5}$  m, bringing the resonant frequency back to the original value.

behavior of  $\mu_{\text{real}}$  and  $\mu_{\text{imag}}$ , dictated by Kramers Kronig, and how resistivity limits the maximum effect achieved.

We next explore the dependence on the radius of the cylinders. In Fig. 11, the radius of the cylinders is decreased, reducing the volume fraction occupied by the cylinders, and raising the resonant frequency by a factor of two. We also decrease  $d$ , the spacing between the sheets, increasing the

capacitance in the system and bringing the resonant frequency back down to its original value.

Using capacitive cylindrical structures such as the Swiss roll structure, we can adjust the magnetic permeability typically by a factor of two and, in addition, if we desire, introduce an imaginary component of the order of unity. The latter implies that an electromagnetic wave moving in such

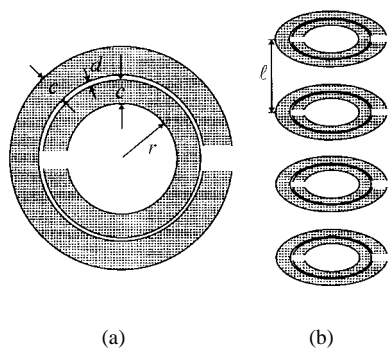


Fig. 12. (a) Plan view of a split ring showing definitions of distances. (b) Sequence of split rings shown in their stacking sequence. Each split ring comprises two thin sheets of metal. The ring shown is a scaled-up version, defined by the parameters shown in Fig. 13.

a material would decay to half its intensity within a single wavelength. This presumes that we are seeking broad-band effects that persist over the greater part of the 2–20-GHz region. However, if we are prepared to settle for an effect over a narrow range of frequencies, spectacular enhancements of the magnetic permeability can be achieved, limited only by the resistivity of the sheets and by how narrow a band we are willing to tolerate.

#### IV. AN ISOTROPIC MAGNETIC MATERIAL

The structures shown above give magnetic properties when the field is aligned along the axes of the cylinders, but have essentially zero magnetic response in other directions. They suffer from another potential problem: if the alternate polarization is considered where the electric field is not parallel to the cylinders, the system responds like an effective metal because current is free to flow along the length of the cylinders. For some applications, this highly anisotropic behavior may be undesirable. Therefore, we redesign the system with a view to restoring isotropy and minimizing purely electrical effects.

To this end, we need a basic unit that is more easily packed into arrays than is a cylinder and that avoids the continuous electrical path provided by a metal cylinder. We propose an adaptation of the “split ring” structure, in which the cylinder is replaced by a series of flat disks each of which retains the “split ring” configuration, but in slightly modified form (see Fig. 12). First, we shall calculate the properties of disks stacked in a square array, as shown in Fig. 13. This structure is still anisotropic, a problem we shall address in a moment, but by eliminating the continuous conducting path that the cylinders provided, it eliminates most of the electrical activity along this direction.

The two-dimensional square array of Fig. 13 can be made by printing with metallic inks. If each printed sheet is then fixed to a solid block of inert material with thickness  $a$ , the blocks can be stacked to give columns of rings. This would establish magnetic activity along the direction of stacking, i.e., the  $z$ -axis. The unit cell of this structure is shown in Fig. 14 on the left-hand side.

How do we make a symmetrical structure? Start from the structure just described, comprising successive layers of rings

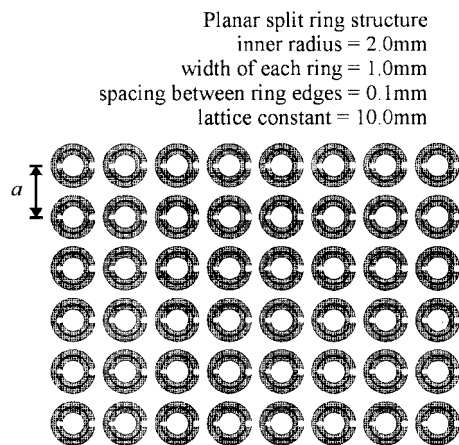


Fig. 13. Plain view of a split ring structure in a square array (lattice spacing  $a$ ).

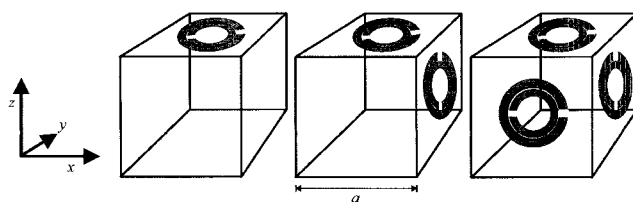


Fig. 14. Building 3-D symmetry: each successive restacking of the structure adds a ring to another side of the unit cell.

stacked along the  $z$ -axis. Next, cut up the structure into a series of slabs thickness  $a$ , make incisions in the  $y$ - $z$ -plane, and be careful to avoid slicing through any of the rings. Each of the new slabs contains a layer of rings, but now each ring is perpendicular to the plane of the slab and is embedded within. Print onto the surface of each slab another layer of rings and stack the slabs back together again. The unit cell of this second structure is shown in the middle of Fig. 14.

In the next step, a third set of slabs is produced by cutting in the  $x$ - $z$ -plane, printing on the surface of the slabs, and reassembling. Finally, we now have a structure with cubic symmetry whose unit cell is shown in the right-hand side of Fig. 14.

Of course, an alternate method of manufacturing this structure would be to start from a set of cubes of the inert material and laboriously stick rings to their sides before assembling the cubes into a lattice. The cut-and-paste method we suggest above is much more efficient.

Now, let us calculate the effective permeability. First, we need to calculate the capacitance between the two elements of the split ring. We shall assume

$$r \gg c \quad r \gg d \quad (39)$$

$$l < r \quad (40)$$

$$\ln \frac{c}{d} \gg \pi. \quad (41)$$

Under these conditions, we can calculate the capacitance between unit length of two parallel sections of the metallic strips

$$C_1 = \frac{\epsilon_0}{\pi} \ln \frac{2c}{d} = \frac{1}{\pi \mu_0 c_0^2} \ln \frac{2c}{d}. \quad (42)$$

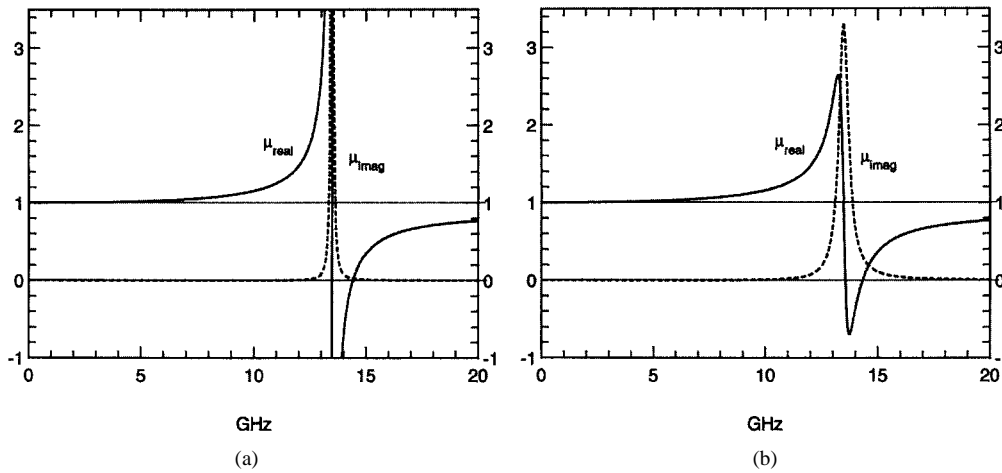


Fig. 15. Plot of  $\mu_{\text{eff}}$  for the cubic split ring structure calculated using the chosen parameters. (a) For copper rings,  $\sigma_1 = 200.0$ . (b) For more resistive rings,  $\sigma_1 = 2000.0$ .

The effective magnetic permeability we calculate, on the assumption that the rings are sufficiently close together and that the magnetic lines of force are due to currents in the stacked rings, are essentially the same as those in a continuous cylinder. This can only be true if the radius of the rings is of the same order as the unit cell side. We arrive at

$$\begin{aligned} \mu_{\text{eff}} &= 1 - \frac{\frac{\pi r^2}{a^2}}{1 + \frac{2\ell\sigma_1}{\omega r\mu_0}i - \frac{3\ell}{\pi^2\mu_0\omega^2 C_1 r^3}} \\ &= 1 - \frac{\frac{\pi r^2}{a^2}}{1 + \frac{2\ell\sigma_1}{\omega r\mu_0}i - \frac{3\ell c_0^2}{\pi\omega^2 \ln \frac{2c}{d} r^3}} \end{aligned} \quad (43)$$

where  $\sigma_1$  is the resistance of unit length of the sheets measured around the circumference.

To give some examples, let us choose a convenient set of parameters

$$\begin{aligned} a &= 1.0 \times 10^{-2} \text{ m} \\ c &= 1.0 \times 10^{-3} \text{ m} \\ d &= 1.0 \times 10^{-4} \text{ m} \\ \ell &= 2.0 \times 10^{-3} \text{ m} \\ r &= 2.0 \times 10^{-3} \text{ m}. \end{aligned} \quad (44)$$

Figs. 12 and 13 show the rings drawn to scale. These parameters do not quite satisfy all the inequalities, which is difficult to do with reasonable numbers, but note that the inequalities are only important to the accuracy of our formulas, not to the functioning of the structure. The resonant frequency at which  $\mu_{\text{eff}}$  diverges is given by

$$\omega_0^2 = \frac{3\ell c_0^2}{\pi \ln \frac{2c}{d} r^3} = 7.1 \times 10^{21} \quad (45)$$

or

$$\omega = 2\pi \times 13.5 \text{ GHz}. \quad (46)$$

If we choose to manufacture the split rings from a layer of copper, it is easily possible to achieve  $\sigma_1 \approx 200.0$ . Evidently, from Fig. 15, this produces a highly resonant structure.

In order to see a substantial effect, we have to increase the resistance either by increasing the resistivity of the material of which the rings are made or by making them thinner.

The scaling of frequency with size can be deduced from (45), in which we see that the resonant frequency scales uniformly with size: if we double the size of all elements in a given structure, the resonant frequency halves. Nearly all the critical properties are determined by this frequency.

## V. ENHANCED NONLINEAR EFFECTS

We have seen how the addition of capacitance to the structure gives a far richer variety of magnetic behavior. Typically, this happens through a resonant interaction between the natural inductance of the structure and the capacitive elements and, at the resonant frequency, electromagnetic energy is shared between the magnetic fields and the electrostatic fields within the capacitive structure. To put this more explicitly, take the split ring structure described in Figs. 12 and 13, most of the electrostatic energy of the capacitor is located in the tiny gap between the rings. Concentrating most of the electromagnetic energy in this very small volume will result in an enormously enhanced energy density.

If we wish to enhance the nonlinear behavior of a given compound, we locate a small amount of the substance in the gap where the strong electrostatic fields are located. Since the response scales as the cube of the field amplitude, we can expect enhancements of the order of the energy density enhancement squared. Furthermore, not only does the structure enhance the nonlinearity, it does so in a manner that is very economical with the material: less than 1% of the structure need be filled with the nonlinear substance.

Note that there is a symmetry between, on the one hand, the present structures designed to generate a magnetic permeability and within which we find enhanced electrostatic fields and, on the other hand, the earlier thin-wire structures [1], [2] designed to generate a negative electrical permittivity, and within which we find enhanced magnetic fields.

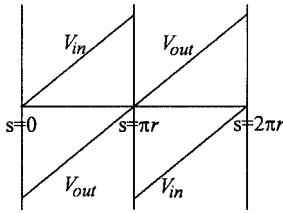


Fig. 16. The emf acting around one of the sheets of the split ring in Fig. 12 as a function of the distance  $s$  around the ring.  $V_{in}$  denotes the emf on the inner ring, and  $V_{out}$  that on the outer ring. Note that this ring is cut at  $s = 0$  so that the emf is discontinuous.

We shall now calculate the energy density in the capacitance between the two split rings in Figs. 12 and 13. First, we calculate the voltage between the two rings as a function of the incident magnetic field  $H_0$ . The electric field between the two halves of the ring is shown in Fig. 16 and is of the order

$$E_{ring} \approx \pi r V_0 d^{-1}. \quad (47)$$

We calculate that

$$V_0 = \frac{3\ell i}{2\omega C_1 \pi^2 r^2} \frac{-H_0}{\left[1 - \frac{\pi r^2}{a^2}\right] + \frac{2\ell\sigma_1 i}{\omega r \mu_0} - \frac{3\ell}{\pi^2 \mu_0 \omega^2 C_1 r^3}}. \quad (48)$$

Hence, on substituting from (42) and (47) into (48)

$$E_{ring} \approx \frac{3\ell \mu_0 c_0^2 i}{2\omega dr \ln \frac{2c}{d}} \frac{-H_0}{\left[1 - \frac{\pi r^2}{a^2}\right] + \frac{2\ell\sigma_1 i}{\omega r \mu_0} - \frac{3\ell c_0^2}{\pi \omega^2 r^3 \ln \frac{2c}{d}}}. \quad (49)$$

We now argue that the electrostatic energy density in the incident electromagnetic field is equal to the magnetic energy density, which, in turn, can be related to the electrostatic energy density in the ring. Hence,

$$\frac{\frac{1}{2}\epsilon_0 |E_{ring}|^2}{\frac{1}{2}\mu_0 |H_{ave}|^2} = \frac{\epsilon_0 \pi^2 r^2 d^{-2}}{\mu_0} \left| \frac{\frac{3\ell}{2\omega C_1 \pi^2 r^2}}{1 + \frac{2\ell\sigma_1 i}{\omega r \mu_0} - \frac{3\ell}{\pi^2 \mu_0 \omega^2 C_1 r^3}} \right|^2. \quad (50)$$

If we evaluate this formula on resonance, we get a much simplified formula as follows:

resonant enhancement

$$= Q = \frac{\frac{1}{2}\epsilon_0 |E_{ring}(\omega_0)|^2}{\frac{1}{2}\mu_0 |H_0(\omega_0)|^2} = \left| \frac{\pi \omega^2 r^3 \mu_0}{4\ell \sigma dc_0} \right|^2. \quad (51)$$

Let us take as an example the following parameters used to calculate Fig. 15:

$$\begin{aligned} d &= 1.0 \times 10^{-4} \text{ m} \\ \ell &= 2.0 \times 10^{-3} \text{ m} \\ r &= 2.0 \times 10^{-3} \text{ m} \\ \sigma_1 &= \frac{R}{ct} = 200.0 \\ \omega_0^2 &= 7.1 \times 10^{21}. \end{aligned} \quad (52)$$

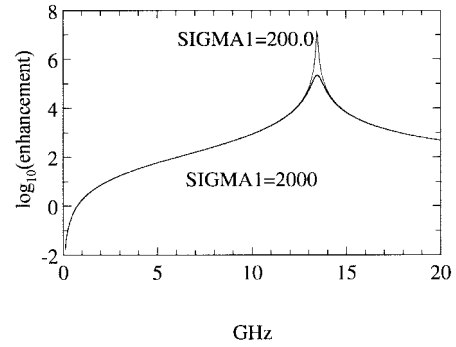


Fig. 17. Enhancement of the energy density of the electric field within the gap between the split rings (see Figs. 12 and 13) for two different values of the resistivity of the metal sheet. The corresponding values of  $\mu_{eff}$  are shown in Fig. 15.

Hence,

$$Q = \left[ \frac{\pi \omega_0^2 r^3 \mu_0}{4\ell \sigma_1 dc_0} \right]^2 = 2.1853 \times 10^7. \quad (53)$$

A more detailed picture of enhancement as a function of frequency is shown in Fig. 17.

For example, a beam of microwaves at 13.41 GHz with power flux of  $10^4 \text{ W}\cdot\text{m}^2$  has an electric field strength of the order of  $2 \times 10^3 \text{ V}\cdot\text{m}^{-1}$  in vacuo. If this beam were incident on, and entirely transmitted into, our magnetic structure, it would generate a field strength of the order of  $10^7 \text{ V}\cdot\text{m}^{-1}$  in the space between the split rings, or of the order of  $10^3 \text{ V}$  between the edges of the two rings: more than enough to cause electrical breakdown in air. It is evident that these structures have considerable potential for enhancing nonlinear phenomena. Furthermore, the nonlinear medium need only be present in the small volume within which the energy is concentrated, opening the possibility of using small quantities of expensive material, and reducing any requirements of mechanical integrity that a larger structure would impose.

In passing, we draw an analogy with surface-enhanced Raman scattering (SERS), observed on rough metallic surfaces—typically silver surfaces. The Raman signal from molecules absorbed on these surfaces may be enhanced by factors of the order of  $10^6$  over that seen on insulating surfaces. The Raman effect is proportional to the second power of the electromagnetic-mode density at the surface, and it is known that roughness can enhance the local-mode density by factors of up to  $10^3$ – $10^4$ , hence, the spectacular Raman enhancement (see [11] for further details and references). A very similar local enhancement takes place in our system and, we expect, can be exploited in an analogous fashion.

In conclusion, we have shown how to design structures made from nonmagnetic thin sheets of metal, which respond to microwave radiation as if they had an effective magnetic permeability. A wide range of permeabilities can be achieved by varying the parameters of the structures. Since the active ingredient in the structure, the metal film, comprises a very small fraction of the volume, typically  $1:10^4$ , the structures may be very light, and reinforced with strong insulating material to ensure mechanical strength, without adversely affecting their magnetic properties. It is likely that the structures will

be exploited for their ability to concentrate the electromagnetic energy in a very small volume, increasing its density by a huge factor, and greatly enhancing any nonlinear effects present.

#### REFERENCES

- [1] J. B. Pendry, A. J. Holden, W. J. Stewart, and I. Youngs, "Extremely low frequency plasmons in metallic meso structures," *Phys. Rev. Lett.*, vol. 76, pp. 4773–4776, 1996.
  - [2] J. B. Pendry, A. J. Holden, D. J. Robbins, and W. J. Stewart, "Low frequency plasmons in thin wire structures," *J. Phys. Condens. Matter*, vol. 10, pp. 4785–4809, 1998.
  - [3] D. F. Sievenpiper, M. E. Sickmiller, and E. Yablonovitch, "3D wire mesh photonic crystals" *Phys. Rev. Lett.*, vol. 76, pp. 2480–2483, 1996.
  - [4] D. F. Sievenpiper, E. Yablonovitch, J. N. Winn, S. Fan, P. R. Villeneuve, and J. D. Joannopoulos, "3D metallo-dielectric photonic crystals with strong capacitive coupling between metallic islands," *Phys. Rev. Lett.*, vol. 80, pp. 2829–2832, 1998.
  - [5] J. B. Pendry "Calculating photonic band structure," *J. Phys. Condens. Matter*, vol. 8, pp. 1085–1108, 1996.
  - [6] D. Pines and D. Bohm, "A collective description of electron interactions: II collective versus individual particle aspects of the interactions," *Phys. Rev.*, vol. 85, pp. 338–353, 1952.
  - [7] D. Bohm and D. Pines, "A collective description of electron interactions: III Coulomb interactions in a degenerate electron gas," *Phys. Rev.*, vol. 92, pp. 609–625, 1953.
  - [8] E. Yablonovitch, "Inhibited spontaneous emission in solid state physics and electronics," *Phys. Rev. Lett.*, vol. 58, pp. 2059–2062, 1987.
  - [9] ———, "Photonic band gap crystals," *J. Phys. Condens. Matter*, vol. 5, pp. 2443–2460, 1993.
  - [10] S. John, "Strong localization of photons in certain disordered lattices," *Phys. Rev. Lett.*, vol. 58, pp. 2486–2489, 1987.
  - [11] F. J. Garcia Vidal and J. B. Pendry, "Collective theory for surface enhanced Raman scattering," *Phys. Rev. Lett.*, vol. 77, pp. 1163–1166, 1996.
  - [12] P. M. Bell, J. B. Pendry, L. Martøn-Moreno, and A. J. Ward, "A program for calculating photonic band structures and transmission coefficients of complex structures," *Comput. Phys. Commun.*, vol. 85, p. 306, 1995.
  - [13] E. Yablonovitch, T. J. Gmitter, and K. M. Leung, "Photonic band structure: The face-centered-cubic case employing nonspherical atoms," *Phys. Rev. Lett.*, vol. 67, pp. 2295–2298, 1991.
  - [14] J. B. Pendry, "Calculating photonic band structure," *J. Phys. Condens. Matter*, vol. 8, pp. 1085–1108, 1996.
  - [15] R. H. Ritchie, "Plasma losses by fast electrons," *Phys. Rev.*, vol. 106, pp. 874–881, 1957.
  - [16] J. B. Pendry and A. MacKinnon, "Calculation of photon dispersion relationships," *Phys. Rev. Lett.*, vol. 69, pp. 2772–2775, 1992.
- J. B. Pendry**, photograph and biography not available at the time of publication.
- A. J. Holden**, photograph and biography not available at the time of publication.
- D. J. Robbins**, photograph and biography not available at the time of publication.
- W. J. Stewart** (M'88), photograph and biography not available at the time of publication.